

Properties of charge transport in a novel holographic quantum phase transition model

Guoyang Fu^{1,*} Huajie Gong^{1,†} Peng Liu^{2,‡} Xiao-Mei Kuang^{1,§} and Jian-Pin Wu^{1,¶}

¹ *Center for Gravitation and Cosmology,
College of Physical Science and Technology,
Yangzhou University, Yangzhou 225009, China and*

² *Department of Physics and Siyuan Laboratory,
Jinan University, Guangzhou 510632, P.R. China*

Abstract

We study the properties of charge transport in a novel holographic QPT (quantum phase transition) model, which has two different metallic phases: the normal metallic phase and the novel metallic one. We numerically work out the scaling behaviors of DC (direct current) resistivity at low temperatures in both different metallic phases. The numerical results are solidly in agreement with the analytical ones determined by the near horizon geometry. Then, we mainly explore the properties of the low-frequency AC (alternating current) conductivity. A remarkable characteristic is that the normal metallic phase is a coherent system with vanishing intrinsic conductivity σ_Q , which is independent of the strength of the momentum dissipation. This result is in contrast with the common belief that with the strength of the momentum dissipation increasing, the system changes from a coherent phase to an incoherent one. But the novel metallic phase is an incoherent system with non-vanishing σ_Q . Away from the QCP (quantum critical point), σ_Q increases, which indicates that the incoherent behavior becomes stronger.

*FuguoyangEDU@163.com

†hua.jiegong@qq.com

‡phylp@email.jnu.edu.cn

§xmeikuang@yzu.edu.cn

¶jianpinwu@yzu.edu.cn

I. INTRODUCTION

AdS/CFT correspondence relates a weakly coupled gravitational theory to a strongly coupled quantum field theory without gravity in the large N limit [1–4]. This duality provides some physical insight into the associated mechanisms of the strongly coupled quantum many-body systems. With the help of AdS/CFT correspondence, significant progresses have been made in understanding novel mechanisms for superconductivity [5] and metal-insulator phase transition (MIT) [6–8], transport properties [9–13], entanglement entropy [14–18], quantum chaos [19–21], and so on.

In holography, the phase is essentially depicted by geometry, such that phase transition is characterized by the transition of geometry [6, 22, 23]. Specifically, the lattice operator in holographic model induces infrared (IR) instability, which leads to a new IR fixed point. The shift between different IR fixed points results in a phase transition. There is also another mechanism driving phase transition. It is the strength of lattice deformation that gives rise to some kind of bifurcating solution such that phase transition happens [6].

MIT, as a prominent example of QPT (quantum phase transition), have been implemented and widely explored from holography [6–8, 22–34]. It is identified by the transition on the sign of slope of the DC (direct-current) conductivity σ_{DC} near extremely low temperature T . Specifically, $\partial_T \sigma_{DC} > 0$ indicates a metallic phase, while $\partial_T \sigma_{DC} < 0$ demonstrates an insulating phase, and $\partial_T \sigma_{DC} = 0$ describes the critical point transiting between the metallic phase and insulating phase.

Recently, we find interesting phenomena in the holographic EMDA (Einstein-Maxwell-dilaton-axions) model [22, 23] that for certain model parameter γ , when we change the lattice parameters, the system exhibits consistent temperature behavior of DC conductivity but with two different IR geometries. According to the geometry viewpoint [6], we argue that there is a novel holographic QPT [23]. We refer to the phase with $\text{AdS}_2 \times \mathbb{R}^2$ IR geometry as the normal metallic phase and the phase with non- $\text{AdS}_2 \times \mathbb{R}^2$ (hyperscaling violation) geometry as the novel metallic phase [23]. It would be interesting to further study the holographic properties of this novel holographic QPT model. Thus, this paper proposes to investigate the charge transport properties by studying DC resistivity and the AC (alternating current) conductivity of the novel state.

We are specially interested in the behavior of the AC conductivity at low frequency as

it can indicate the metal in a coherent phase or an incoherent one. Usually, for a coherent metallic phase, the behavior of the AC conductivity at low frequency is fitted by the standard Drude formula

$$\sigma(\omega) = \frac{\sigma_{DC}}{1 - i\omega\tau}, \quad (1)$$

with τ the relaxation time, which depends on the temperature, and if the above formula is violated, the corresponding metal could be in an incoherent phase. In holographic framework, it is common that the dual metal phase could transit between coherent and incoherent phases. For instance, in the Einstein-Maxwell-axions (EMA) theory or Gubser-Rocha-axions model [35, 36], the standard Drude formula (1) was found to be satisfied only when momentum dissipation of system is weak. But as the momentum dissipation enhances, the low-frequency behavior of AC conductivity cannot be fitted by (1), implying that the metal is in incoherent phase, which is depicted by the modified Drude formula [35, 36]

$$\sigma(\omega) = \frac{\sigma_{DC} - \sigma_Q}{1 - i\omega\tau} + \sigma_Q, \quad (2)$$

where σ_Q is known as the intrinsic conductivity [37]. From the modified Drude formula (2), the low-frequency conductivity for incoherent metallic phases attributes to two compositions: the coherent contribution due to momentum relaxation and the incoherent contribution due to the intrinsic current relaxation. Since we could expect that the charge transport behaviors in the normal and novel metallic phases we found in holographic EMDA model [23] could be different, the careful study on the AC conductivity at low frequency could help to further understand the normal and novel phases.

We organize the paper as follows. In section II, we review the holographic EMDA model proposed in [22, 23]. Then, in section III, we calculate the DC resistivity and study its scaling behavior at low temperatures. Section IV is dedicated to the properties of low-frequency AC conductivities. Finally, in section V, we conclude the paper by presenting a summary and a discussion.

II. HOLOGRAPHIC SETUP

In this section, we briefly review the holographic setup of EMDA model. For the details, please refer to Refs.[22, 23]. The EMDA action we considered is [22, 23]

$$S = \int d^4x \sqrt{-g} \left[R + 6 \cosh \psi - \frac{3}{2} [(\partial\psi)^2 + 4 \sinh^2 \psi (\partial\chi)^2] - \frac{1}{4} \cosh^{\gamma/3} (3\psi) F^2 \right], \quad (3)$$

where we have fixed the *AdS* radius $L = 1$. ψ is the dilaton field coupled with the Maxwell field $F \equiv dA$ and the axion field χ . γ is the coupling parameter. Depending on this coupling parameter, the system exhibits appealing landscapes of holographic QPT as illustrated in Refs.[22, 23]. We are interested in the novel QPT, which changes from a normal metallic phase to a novel metallic one when γ in the region of $\gamma > 3$. Without loss of generality, we set $\gamma = 9/2$ through this paper.

To solve this holographic system (3), we assume the following ansatz

$$\begin{aligned} ds^2 &= \frac{1}{z^2} \left[- (1-z)p(z)U(z)dt^2 + \frac{dz^2}{(1-z)p(z)U(z)} + V_1(z)dx^2 + V_2(z)dy^2 \right], \quad (4) \\ A &= \mu(1-z)a(z)dt, \\ \psi &= z^{3-\Delta}\phi(z), \\ \chi &= \hat{k}x, \end{aligned}$$

where $p(z) = 1+z+z^2 - \mu^2 z^3/4$, \hat{k} is the charge of the axion field, which depicts the strength of momentum dissipation, and μ is interpreted as the chemical potential. In our model (3), the conformal dimension of the dilaton field is $\Delta = 2$.

The action (3) with the ansatz (4) gives four second order ordinary differential equations (ODEs) for V_1, V_2, a, ϕ and one first order ODE for U . The asymptotic AdS_4 on the conformal boundary require that

$$U(0) = 1, \quad V_1(0) = 1, \quad V_2(0) = 1, \quad a(0) = 1, \quad \phi(0) = \hat{\lambda}, \quad (5)$$

where $\hat{\lambda}$ is the source of the dilaton field operator in the dual field theory and characterizes the lattice deformation. Collecting all the above information with the regular boundary conditions at the horizon, we can solve this holographic system numerically.

The Hawking temperature of black hole is

$$\hat{T} = \frac{(12 - \mu^2)U(1)}{16\pi}, \quad (6)$$

which is considered as the temperature of the dual theory. We set the chemical potential μ as the scaling unit as our previous work [23] and this system is described by the three dimensionless parameters $\{T, \lambda, k\} \equiv \{\hat{T}/\mu, \hat{\lambda}/\mu, \hat{k}/\mu\}$.

III. DC RESISTIVITY

In this section, we shall mainly investigate the properties of DC resistivity of the novel metallic phase. We shall employ the scheme proposed in [22] (also see [30, 38]) to calculate the DC resistivity. To proceed, we turn on the following perturbations:

$$\begin{aligned} g_{tx} &= \delta h_{tx}(z), & g_{xz} &= \delta h_{xz}(z), \\ A_x &= -E_x t + \delta a_x(z), & \chi &= kx + \delta \chi(z), \end{aligned} \quad (7)$$

where E_x is the constant electric field along x direction. Then we find the conserved current \mathcal{J} in the bulk:

$$\mathcal{J} = \sqrt{\frac{V_2(z)}{V_1(z)}} Z(\psi(z)) (z^2 \delta h_{tx}(z) A'(z) + f(z) \delta a'_x(z)), \quad (8)$$

which is the key point of this method. In order to ensure the regularity of the metric field and the gauge field at the horizon, we have the solutions from boundary conditions as

$$\delta h_{tx}(z) = -f(z) \delta h_{xz}(z), \quad \delta a'_x(z) = \frac{E_x}{f(z)}, \quad (9)$$

where $f(z) = (1-z)p(z)U(z)$ and $Z(\psi(z)) = \cosh^{\gamma/3}(3\psi(z))$. Substituting the above equations into the conserved current \mathcal{J} we constructed, we obtain the expression of DC resistivity as

$$\rho = \left(\sqrt{\frac{V_2}{V_1}} \left(\cosh^{\gamma/3}(3\phi) + \frac{V_1 a^2 \cosh^{2/3\gamma}(3\phi)}{12k^2 \sinh^2(\phi)} \right) \right)^{-1} \Big|_{z \rightarrow 1}. \quad (10)$$

Once the background solution is numerically worked out, we can obtain the DC resistivity in terms of the above expression.

Fig.1 shows the DC resistivity ρ as the function of the temperature for different k . Left plot is for the normal metallic phase, while the right one is the novel metallic phase. As expected, for the normal metallic phase, the DC resistivity decreases with the temperature.

In the novel metallic phase, the results are completely different. When k is small, the DC resistivity decreases with the temperature, which is obviously metallic behavior. While

for large k (for example, $k = 0.8$, see the right plot in Fig.1), as the temperature decreases, the DC resistivity rises up at first, which exhibits an insulating behavior, and then decreases, which indicates a metallic behavior. However, at extremally low temperature, this holographic system indeed exhibits metallic behavior.

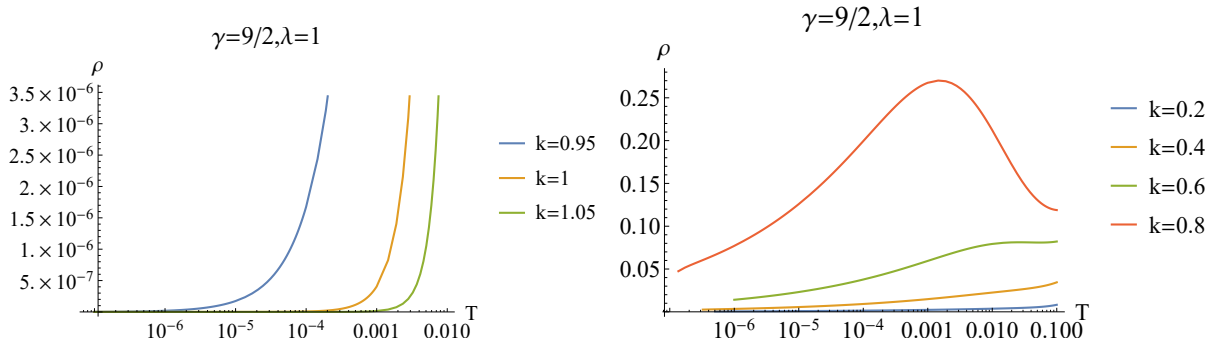


FIG. 1: Semilogarithmic plots of DC resistivity ρ as the function of the temperature for different k . Here we fix $\gamma = 9/2$ and $\lambda = 1$. The left plot is for the normal metallic phase, while the right one is the novel metallic phase.

To roughly check our numerical results, we shall further extract the scaling behavior of the DC resistivity at low temperature from our numerical results and then compare with the analytical results found in Ref.[22] which is found to be determined by the near horizon geometry.

In order to compare explicitly, we first briefly review the analytical results of Ref.[22]. We start with the novel metallic phase. Its IR geometry is the hyperscaling violation one:

$$ds^2 = L^{-2}r^{u_1}dt^2 + L^2r^{-u_1}dr^2 + e^{v_{10}}r^{2v_{11}}dx^2 + e^{v_{20}}r^{2v_{22}}dy^2, \quad (11)$$

$$A_t = a_0r^{a_1}, \quad e^\phi = e^{\phi_0}r^{\phi_1},$$

where the radial exponents are [22]

$$u_1 = \frac{2(10 + 3\gamma + \gamma^2)}{11 + 4\gamma + \gamma^2}, \quad v_{11} = -\frac{1 + \gamma}{11 + 4\gamma + \gamma^2}, \quad v_{22} = \frac{(1 + \gamma)(2 + \gamma)}{11 + 4\gamma + \gamma^2},$$

$$a_1 = \frac{2(5 + 2\gamma + \gamma^2)}{11 + 4\gamma + \gamma^2}, \quad \phi_1 = -\frac{2(1 + \gamma)}{11 + 4\gamma + \gamma^2}. \quad (12)$$

v_{10} , v_{20} , a_0 and ϕ_0 are determined by the IR geometry datas, which can be numerically worked out. Combining Eqs.(11) and (12) with Eq.(10), we find that both terms of Eq.(10) follow the same scaling behaviors [22]

$$\rho \sim T^{-\frac{(1+\gamma)(3-\gamma)}{9+2\gamma+\gamma^2}}. \quad (13)$$

It is found that in the novel metallic phase, the scaling exponent only depends on the parameter γ and is independent of the strength of momentum dissipation k .

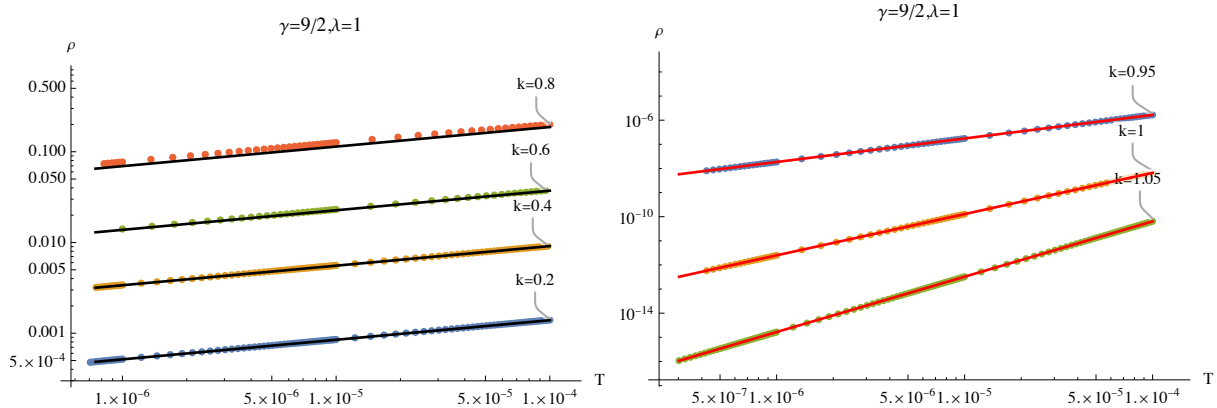


FIG. 2: The log-log plot of the DC resistivity ρ as the function of temperature T for different k . The left plot is for the novel metallic phase, while the right plot for the normal metallic one. The dots are the numerical results and the solid lines are the analytical ones, which are evaluated by Eq.(13) and Eq.(14), respectively.

The left plot in Fig.2 shows the log-log plot of the DC resistivity as the function of temperature in the novel metallic phase. The dots are the numerical results and the solid lines are the analytical ones, which are evaluated by Eq.(13). It is clearly seen that the numerical results are in good agreement with the analytical ones. Quantitatively, we also fit the numerical data with the form of $\rho \sim T^\alpha$. The fitting results are summarized in Table I. On the other hand, since through this paper, we fix $\gamma = 9/2$, the scaling exponent can be evaluated by Eq.(13) as $\alpha \approx 0.21569$. Again, the quantitative numerical results are well consistent with the analytical ones determined by Eq.(13).

TABLE I: The scaling exponents fitted with the form of $\rho \sim T^\alpha$ in the novel metallic phase.

k	0.200	0.400	0.600	0.800
α	0.21519	0.21517	0.21394	0.20756

Now, we turn to the case of the normal metallic phase, whose IR geometry is $\text{AdS}_2 \times \mathbb{R}^2$. Especially, the value of the dilaton field ϕ tends to zero near the horizon. In this case, the second term in Eq.(10) dominates over the first term. Therefore, the DC resistivity follows

$$\rho \sim T^{2\delta\phi}, \quad (14)$$

with

$$\delta\phi = -\frac{1}{2} + \frac{1}{6}\sqrt{24e^{2v_{10}}k^2 - 3(12\gamma + 1)}. \quad (15)$$

It is found that different from the novel metallic phase, now the scaling exponent obviously depends on the strength of the momentum dissipation k , and also depends on v_{10} , which is determined by the IR geometry data and need to be numerically worked out. We show the log-log plot of the DC resistivity as the function of temperature in the normal metallic phase in the right plot in Fig.2 and also fit its scaling exponent in Table II. The numerical results are highly consistent with that evaluated in terms of Eq.(14) and Eq.(15).

TABLE II: The scaling exponent α_1 is fitted with the form of $\rho \sim T^{\alpha_1}$ in the normal metallic phase. $\alpha_2 \equiv 2\delta\phi$ is evaluated in terms of Eq.(15).

k	0.950	1.000	1.050
α_1	0.97628	1.71033	2.29306
α_2	0.97083	1.70567	2.28942

In this section, we have numerically worked out the scaling behavior of the DC resistivity at low temperature. The numerical results are solidly in agreement with the analytical ones, which are determined by the IR geometry. It also indicated that the numerics we implemented here are robust at the extremal low temperatures. The numerical techniques provide us with powerful techniques to deal with the AC conductivities at low temperatures in the next section, which is a hard task to handle especially at extremally low temperature.

IV. AC CONDUCTIVITY

In this section, we study the properties of the AC conductivity over the EMDA background along the direction of lattice, i.e., x -direction here. To this end, we turn on the following consistent linear perturbations

$$g_{tx} = e^{-i\omega t}\delta h_{tx}(z), \quad A_x = e^{-i\omega t}\delta a_x(z), \quad \chi = e^{-i\omega t}\delta\chi(z). \quad (16)$$

Then we obtain three coupling perturbative equations for $\delta h_{tx}(z)$, $\delta a_x(z)$ and $\delta\chi(z)$.

Without loss of generality, we set $\delta a_x(0) = 1$ at the UV boundary ($z = 0$), which provides the source of the gauge field. To guarantee what we extract is the current-current correlator

of the dual boundary field theory, we need to impose the boundary condition as $\delta\chi(0) - ik\delta h_{tx}(0)/\omega = 0$ at the UV boundary, which comes from the diffeomorphism and gauge transformation. At the horizon, we shall impose the ingoing boundary conditions. Once the perturbative equations are worked out numerically, we can read off the AC conductivity along x -direction by

$$\sigma(\omega) = \frac{\partial_z \delta a_x(z)}{i\omega \delta a_x(z)} \Big|_{z \rightarrow 0}. \quad (17)$$

Fig.3 shows the AC conductivity as a function of frequency for different k . The conductivity tends to a constant in the high frequency limit ($\omega \gg \mu$), which is determined by ultra-violet (UV) AdS₄ fixed point. More rich physics lies at the low frequency region.

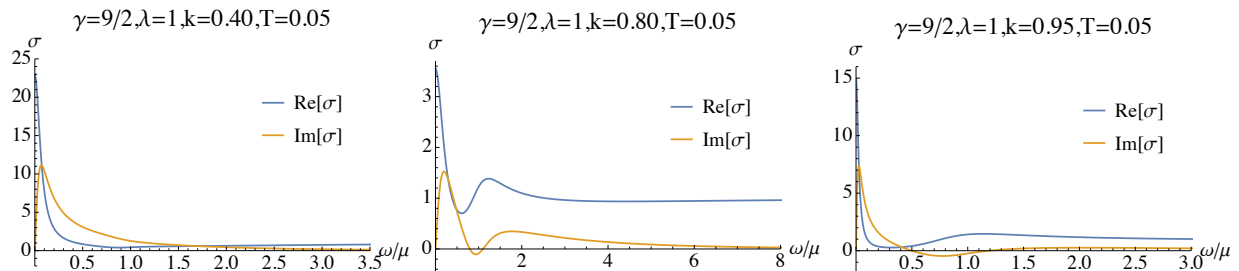


FIG. 3: AC conductivity as a function of frequency for different $k = 0.40, 0.80, 0.95$ (from left to right). The temperature is fixed at $T=0.05$.

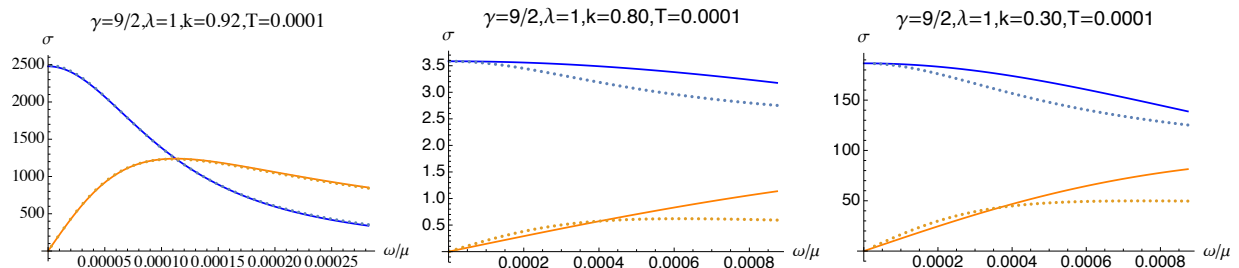


FIG. 4: AC conductivity as a function of frequency for different $k = 0.92, 0.80, 0.30$ (from left to right) at $T = 0.0001$. The dots are the numerical results while the solid lines are fitted by the standard Drude formula (1).

Firstly, we try to fit the low-frequency AC conductivity at extremal low temperature ($T = 0.0001$) by the standard Drude formula (1). As expected, for the normal metallic phase, the AC conductivity at low frequency can be well fitted by the standard Drude

formula (the first plot in Fig.4). However, if the system is in the novel metallic phase, the standard Drude formula is violated (the second and third plots in Fig.4). This observation prompts us to resort to a modified Drude formula, and we shall again borrow the modified Drude formula (2).

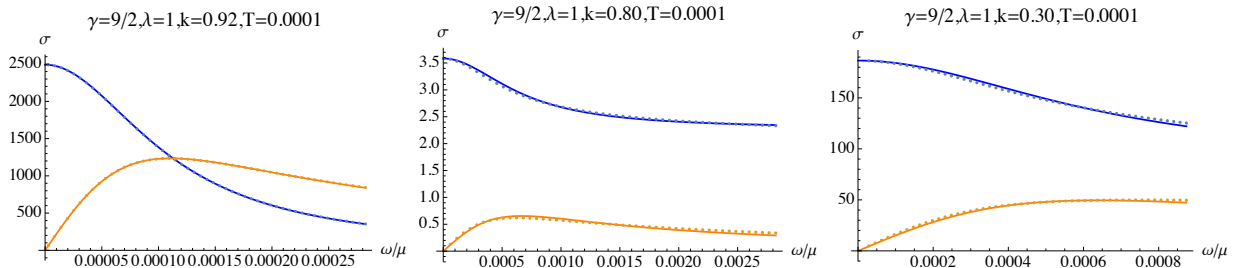


FIG. 5: AC conductivity as a function of frequency for different $k = 0.92, 0.80, 0.30$ (from left to right) at $T = 0.0001$. The dots are the numerical results while the solid lines are fitted by the modified Drude formula (2).

TABLE III: Fitting parameters τ and σ_Q for different k at $T = 0.0001$.

k	0.300	0.500	0.800	0.820	0.840	0.920	0.922	0.930	0.940
$\tau\mu$	1559.98	1592.79	1626.28	1709.91	1834.11	8941.24	12464.02	42898.94	175256.74
σ_Q	87.493	20.709	2.325	1.946	1.625	0	0	0	0

Fig.5 shows the fitting plots by the modified Drude formula (2). We find that whether in the normal metallic phase or in the novel metallic phase, the AC conductivity can be well fitted by the modified Drude formula (2). Quantitatively, we show the fitting parameters τ and σ_Q in Table III. The main characteristics are summarized as follows.

- In the normal metallic phase, $\sigma_Q = 0$. It indicates that this metallic phase is the coherent one, which is independent of the strength of the momentum dissipation k . It is different from the usual EMA model or Gubser-Rocha-axions model, where with the strength of the momentum dissipation increases, the system changes from coherent phase to incoherent one [35, 36, 39, 40].
- The novel metallic phase has non-vanishing σ_Q , which suggests an incoherent behavior. Deviating from the quantum critical point (QCP), σ_Q increases. It means that the incoherent behavior becomes stronger.

- Whether in the normal metallic phase or in the novel metallic one, the relaxation time increases as the momentum dissipation enhances, which is consistent with that of the usual holographic axions model [39, 41].

In conclusion, there are obvious differences in the low-frequency AC conductivities between the normal metallic phase and the novel metallic one. These differences attribute to the different IR geometries of the two phases. We expect to reveal the mechanisms underlying these characteristics of AC conductivity in near future. At least, there are two possible ways to achieve this end. Following the method in [35, 36], we can test the robustness of the modified Drude formula (2). Especially, it maybe addresses what determines the relaxation time τ and the intrinsic conductivity σ_Q in this model. But to derive the low-frequency AC conductivity behavior, the key point is to decouple the linearized perturbative equations, which is a hard work in our model. We can refer to the work [36] for detailed discussions. Another possible way to analytically work out the low-frequency AC conductivity is the so-called matching method, which have been widely used in holography, see for example [40, 42–49].

V. CONCLUSION AND DISCUSSION

In this paper, we study the properties of charge transport on a special EMDA theory [22, 23]. We specially focus on the novel metallic state, which has two different metallic phases: the normal metallic phase and the novel metallic phase [22, 23]. We numerically study the scaling behaviors of two different metallic phases. The numerical results are excellently consistent with the analytical ones determined by the near horizon geometry [22].

We mainly focused on the low-frequency behaviors of AC conductivity in the two different metallic phases. We assume the modified Drude formula (2), derived in the holographic dual system of EMA theory and Gubser-Rocha-axions model [35, 36], is universal and also applicable to our present novel metallic state. A remarkable characteristic is that the normal metallic phase is a coherent system with vanishing intrinsic conductivity σ_Q , which is independent of the strength of the momentum dissipation. As we all know, the usual axions dual system changes from a coherent phase to an incoherent one with the strength of the momentum dissipation increasing. But the novel metallic phase is an incoherent sys-

tem with non-vanishing σ_Q . Away from the QCP, σ_Q increases, which indicates that the incoherent behavior becomes stronger. These differences between the two phases can be attributed to the different IR geometries. We expect to reveal the mechanisms underlying these characteristics of AC conductivity in near future.

The special EMDA model proposed in [22, 23] provides a platform to study the QPT. There are lots of directions deserving further exploration. We can study the quantum information measurement including the holographic entanglement entropy and the entanglement wedge minimum cross-section in this EMDA model following the idea in [30, 50, 51]. It is also worthwhile to study the properties of AC conductivity in other states, especially the insulating phases, which have been revealed in [23]. Moreover, we would like to construct the anisotropic background based on this EMDA model such that we can study its dynamical properties. Such dynamical properties have been explored in the anisotropic background based on the Q-lattice model [52].

Acknowledgments

This work is supported by the Natural Science Foundation of China under Grant Nos. 11905083, 11775036, 12147209, the Postgraduate Research & Practice Innovation Program of Jiangsu Province under Grant Nos. KYCX20_2973 and KYCX22_3451, Fok Ying Tung Education Foundation under Grant No. 171006, Natural Science Foundation of Jiangsu Province under Grant No. BK20211601, and Top Talent Support Program from Yangzhou University.

-
- [1] J. M. Maldacena, *The Large N limit of superconformal field theories and supergravity*, Adv. Theor. Math. Phys. **2** (1998) 231–252, [[hep-th/9711200](#)].
 - [2] S. S. Gubser, I. R. Klebanov, and A. M. Polyakov, *Gauge theory correlators from noncritical string theory*, Phys. Lett. B **428** (1998) 105–114, [[hep-th/9802109](#)].
 - [3] E. Witten, *Anti-de Sitter space and holography*, Adv. Theor. Math. Phys. **2** (1998) 253–291, [[hep-th/9802150](#)].
 - [4] O. Aharony, S. S. Gubser, J. M. Maldacena, H. Ooguri, and Y. Oz, *Large N field theories, string theory and gravity*, Phys. Rept. **323** (2000) 183–386, [[hep-th/9905111](#)].

- [5] S. A. Hartnoll, C. P. Herzog, and G. T. Horowitz, *Building a Holographic Superconductor*, Phys. Rev. Lett. **101** (2008) 031601, [[arXiv:0803.3295](#)].
- [6] A. Donos and S. A. Hartnoll, *Interaction-driven localization in holography*, Nature Phys. **9** (2013) 649–655, [[arXiv:1212.2998](#)].
- [7] Y. Ling, C. Niu, J. Wu, Z. Xian, and H.-b. Zhang, *Metal-insulator Transition by Holographic Charge Density Waves*, Phys. Rev. Lett. **113** (2014) 091602, [[arXiv:1404.0777](#)].
- [8] Y.-S. An, T. Ji, and L. Li, *Magnetotransport and Complexity of Holographic Metal-Insulator Transitions*, JHEP **10** (2020) 023, [[arXiv:2007.13918](#)].
- [9] S. A. Hartnoll, *Lectures on holographic methods for condensed matter physics*, Class. Quant. Grav. **26** (2009) 224002, [[arXiv:0903.3246](#)].
- [10] M. Natsuume, *AdS/CFT Duality User Guide*, [arXiv:1409.3575](#).
- [11] S. A. Hartnoll, A. Lucas, and S. Sachdev, *Holographic quantum matter*, [arXiv:1612.07324](#).
- [12] M. Baggioli, *Applied Holography: A Practical Mini-Course*, [arXiv:1908.02667](#).
- [13] M. Baggioli, K.-Y. Kim, L. Li, and W.-J. Li, *Holographic Axion Model: a simple gravitational tool for quantum matter*, Sci. China Phys. Mech. Astron. **64** (2021), no. 7 270001, [[arXiv:2101.01892](#)].
- [14] S. Ryu and T. Takayanagi, *Holographic derivation of entanglement entropy from AdS/CFT*, Phys. Rev. Lett. **96** (2006) 181602, [[hep-th/0603001](#)].
- [15] T. Takayanagi, *Entanglement Entropy from a Holographic Viewpoint*, Class. Quant. Grav. **29** (2012) 153001, [[arXiv:1204.2450](#)].
- [16] A. Lewkowycz and J. Maldacena, *Generalized gravitational entropy*, JHEP **08** (2013) 090, [[arXiv:1304.4926](#)].
- [17] V. E. Hubeny, M. Rangamani, and T. Takayanagi, *A Covariant holographic entanglement entropy proposal*, JHEP **07** (2007) 062, [[arXiv:0705.0016](#)].
- [18] X. Dong, A. Lewkowycz, and M. Rangamani, *Deriving covariant holographic entanglement*, JHEP **11** (2016) 028, [[arXiv:1607.07506](#)].
- [19] A. Kitaev, *Hidden correlations in the Hawking radiation and thermal noise*, talk given at the Fundamental Physics Prize Symposium (Nov. 10, 2014).
- [20] J. Maldacena, S. H. Shenker, and D. Stanford, *A bound on chaos*, JHEP **08** (2016) 106, [[arXiv:1503.01409](#)].
- [21] D. A. Roberts and B. Swingle, *Lieb-Robinson Bound and the Butterfly Effect in Quantum*

- Field Theories*, Phys. Rev. Lett. **117** (2016), no. 9 091602, [[arXiv:1603.09298](#)].
- [22] A. Donos and J. P. Gauntlett, *Novel metals and insulators from holography*, JHEP **06** (2014) 007, [[arXiv:1401.5077](#)].
- [23] G. Fu, X.-J. Wang, P. Liu, D. Zhang, X.-M. Kuang, and J.-P. Wu, *A novel holographic quantum phase transition and butterfly velocity*, JHEP **04** (2022) 148, [[arXiv:2202.01495](#)].
- [24] A. Donos, B. Goutéraux, and E. Kiritsis, *Holographic Metals and Insulators with Helical Symmetry*, JHEP **09** (2014) 038, [[arXiv:1406.6351](#)].
- [25] A. Donos and J. P. Gauntlett, *Holographic Q-lattices*, JHEP **04** (2014) 040, [[arXiv:1311.3292](#)].
- [26] M. Baggioli and O. Pujolas, *Electron-Phonon Interactions, Metal-Insulator Transitions, and Holographic Massive Gravity*, Phys. Rev. Lett. **114** (2015), no. 25 251602, [[arXiv:1411.1003](#)].
- [27] E. Kiritsis and J. Ren, *On Holographic Insulators and Supersolids*, JHEP **09** (2015) 168, [[arXiv:1503.03481](#)].
- [28] Y. Ling, P. Liu, C. Niu, and J.-P. Wu, *Building a doped Mott system by holography*, Phys. Rev. D **92** (2015), no. 8 086003, [[arXiv:1507.02514](#)].
- [29] Y. Ling, P. Liu, and J.-P. Wu, *A novel insulator by holographic Q-lattices*, JHEP **02** (2016) 075, [[arXiv:1510.05456](#)].
- [30] Y. Ling, P. Liu, J.-P. Wu, and Z. Zhou, *Holographic Metal-Insulator Transition in Higher Derivative Gravity*, Phys. Lett. B **766** (2017) 41–48, [[arXiv:1606.07866](#)].
- [31] E. Mefford and G. T. Horowitz, *Simple holographic insulator*, Phys. Rev. D **90** (2014), no. 8 084042, [[arXiv:1406.4188](#)].
- [32] M. Baggioli and O. Pujolas, *On Effective Holographic Mott Insulators*, JHEP **12** (2016) 107, [[arXiv:1604.08915](#)].
- [33] T. Andrade, A. Krikun, K. Schalm, and J. Zaanen, *Doping the holographic Mott insulator*, Nature Phys. **14** (2018), no. 10 1049–1055, [[arXiv:1710.05791](#)].
- [34] S. Bi and J. Tao, *Holographic DC conductivity for backreacted NLED in massive gravity*, JHEP **06** (2021) 174, [[arXiv:2101.00912](#)].
- [35] R. A. Davison and B. Goutéraux, *Dissecting holographic conductivities*, JHEP **09** (2015) 090, [[arXiv:1505.05092](#)].
- [36] Z. Zhou, Y. Ling, and J.-P. Wu, *Holographic incoherent transport in*

- Einstein-Maxwell-dilaton Gravity*, Phys. Rev. D **94** (2016), no. 10 106015, [[arXiv:1512.01434](#)].
- [37] R. A. Davison, B. Goutéraux, and S. A. Hartnoll, *Incoherent transport in clean quantum critical metals*, JHEP **10** (2015) 112, [[arXiv:1507.07137](#)].
- [38] M. Blake and A. Donos, *Quantum Critical Transport and the Hall Angle*, Phys. Rev. Lett. **114** (2015), no. 2 021601, [[arXiv:1406.1659](#)].
- [39] T. Andrade and B. Withers, *A simple holographic model of momentum relaxation*, JHEP **05** (2014) 101, [[arXiv:1311.5157](#)].
- [40] R. A. Davison, *Momentum relaxation in holographic massive gravity*, Phys. Rev. D **88** (2013) 086003, [[arXiv:1306.5792](#)].
- [41] J.-P. Wu, X.-M. Kuang, and Z. Zhou, *Holographic transports from Born–Infeld electrodynamics with momentum dissipation*, Eur. Phys. J. C **78** (2018), no. 11 900, [[arXiv:1805.07904](#)].
- [42] T. Faulkner, H. Liu, J. McGreevy, and D. Vegh, *Emergent quantum criticality, Fermi surfaces, and AdS2*, Phys. Rev. D **83** (2011) 125002, [[arXiv:0907.2694](#)].
- [43] N. Iqbal, H. Liu, and M. Mezei, *Lectures on holographic non-Fermi liquids and quantum phase transitions*, in Theoretical Advanced Study Institute in Elementary Particle Physics: String theory and its Applications: From meV to the Planck Scale, pp. 707–816, 10, 2011. [[arXiv:1110.3814](#)].
- [44] J.-P. Wu, *Holographic fermions on a charged Lifshitz background from Einstein-Dilaton-Maxwell model*, JHEP **03** (2013) 083.
- [45] J.-P. Wu, *The analytical treatments on the low energy behaviors of the holographic non-relativistic fermions*, Phys. Lett. B **723** (2013) 448–454.
- [46] X.-M. Kuang and J.-P. Wu, *Analytical shear viscosity in hyperscaling violating black brane*, Phys. Lett. B **773** (2017) 422–427, [[arXiv:1511.03008](#)].
- [47] Y. Liu, K. Schalm, Y.-W. Sun, and J. Zaanen, *Lattice Potentials and Fermions in Holographic non Fermi-Liquids: Hybridizing Local Quantum Criticality*, JHEP **10** (2012) 036, [[arXiv:1205.5227](#)].
- [48] M. Edalati, J. I. Jottar, and R. G. Leigh, *Transport Coefficients at Zero Temperature from Extremal Black Holes*, JHEP **01** (2010) 018, [[arXiv:0910.0645](#)].
- [49] R.-G. Cai, Y. Liu, and Y.-W. Sun, *Transport Coefficients from Extremal Gauss-Bonnet*

- Black Holes*, JHEP **04** (2010) 090, [[arXiv:0910.4705](#)].
- [50] Y. Ling, P. Liu, C. Niu, J.-P. Wu, and Z.-Y. Xian, *Holographic Entanglement Entropy Close to Quantum Phase Transitions*, JHEP **04** (2016) 114, [[arXiv:1502.03661](#)].
- [51] Y. Ling, P. Liu, and J.-P. Wu, *Characterization of Quantum Phase Transition using Holographic Entanglement Entropy*, Phys. Rev. D **93** (2016), no. 12 126004, [[arXiv:1604.04857](#)].
- [52] P. Liu and J.-P. Wu, *Dynamic properties of two-dimensional latticed holographic system*, JHEP **02** (2022) 119, [[arXiv:2104.04189](#)].